The elastocapillary Landau–Levich problem

Harish N. Dixit† and G. M. Homsy

Department of Mathematics, University of British Columbia, 1984 Mathematics Road,
Vancouver, BC, V6T 1Z2, Canada

We study the classical Landau–Levich dip-coating problem for the case in which the interface possesses both elasticity and surface tension. The aim of the study is to develop a complete asymptotic theory of the elastocapillary Landau–Levich problem in the limit of small flow speeds. As such, the paper also extends our previous study on purely elastic Landau–Levich flow (Dixit & Homsy *J. Fluid Mech.*, vol. 732, 2013, pp. 5–28) to include the effect of surface tension. The elasticity of the interface is described by the Helfrich model and surface tension is modelled in the usual way. We define an elastocapillary number, ϵ, which represents the relative strength of elasticity to surface tension. Based on the size of ϵ, we can define three different regimes of interest. In each of these regimes, we carry out asymptotic expansions in the small capillary (or elasticity) numbers, which represents the balance of viscous forces to surface tension (or elasticity).

In the weak elasticity regime, the film thickness is a small correction to the classical Landau–Levich law and can be written as

$$\tilde{h}_{\infty,c} = (0.9458 - 0.0839\,\mathscr{E})l_c Ca^{2/3}, \quad \epsilon \ll 1,$$

where l_c is the capillary length, Ca is the capillary number and $\mathscr{E} = \epsilon/Ca^{2/3}$. In the elastocapillary regime, the film thickness is a function of ϵ through the power-law relationship

$$\tilde{h}_{\infty,ec} = \bar{h}_{\infty,e} L f(\epsilon) Ca^{4/7}, \quad \epsilon \sim O(1),$$

where $\bar{h}_{\infty,e}$ is a numerical coefficient obtained in our previous study, L is the elastocapillary length, and $f(\epsilon)$ represents the functional dependence of film thickness on the elastocapillary parameter.

Key words: coating, lubrication theory, capillary flows

---

1. Introduction

In a previous paper, Dixit & Homsy (2013), we studied the effect of interfacial elasticity on the classical Landau–Levich dip-coating flow in the absence of surface tension. The results obtained in that analysis have motivated a detailed investigation of the relative roles of surface tension and elasticity in the Landau–Levich problem. We

† Present address: Department of Mechanical Engineering, Indian Institute of Technology Hyderabad, Yeddumailaram, Andhra Pradesh, India - 502205. Email address for correspondence: hdixit@iith.ac.in

therefore first summarize key results from that paper and then discuss the scope of the present paper.

In the classical Landau–Levich dip-coating flow, the film thickness, $\tilde{h}_{\infty,c}$, varies as a function of the capillary number according to the relation

$$\tilde{h}_{\infty,c} = 0.9458 l_c Ca^{2/3}, \tag{1.1}$$

where $l_c = \sqrt{\sigma/\rho g}$ is the capillary length, ρ is the density of the underlying fluid, g is the acceleration due to gravity, and $Ca = \mu U/\sigma$ is the capillary number with U, μ and σ being the velocity of withdrawal of the plate, viscosity and surface tension respectively. The subscript c in $\tilde{h}_{\infty,c}$ denotes that the above result is valid for a clean interface possessing a constant surface tension. If the fluid interface is replaced with an elastic membrane, then (1.1) is replaced with the following result, valid in the absence of surface tension (Dixit & Homsy 2013):

$$\tilde{h}_{\infty,e} = \bar{h}_{\infty,e} l_e El^{4/7}, \tag{1.2}$$

where $El = \mu U l_e^2/K_B$ is the elasticity number, $l_e = (K_B/\rho g)^{1/4}$ is the elasticity length, K_B is the bending stiffness of the elastic interface, and $\bar{h}_{\infty,e}$ is a numerical coefficient. Equation (1.2) is the key result in Dixit & Homsy (2013). A remarkable feature of this result is that unlike the classical Landau–Levich result, $\bar{h}_{\infty}$ is not unique. In Dixit & Homsy (2013), we identify at least five solutions, i.e. five values of $\bar{h}_{\infty}$. To obtain the above result, the flow field was divided into two regions: a static region where elasticity balances gravity and a transition region where elasticity balances viscous forces. Solutions in the two regions were matched using the method of matched asymptotic expansions. The main goal of the present paper is to rationalize the two results, (1.1) and (1.2). Therefore, we develop an elastocapillary theory where the interface possesses both elasticity and surface tension.

In addition to the primary objective of rationalizing the difference between (1.1) and (1.2) from a theoretical perspective, the current work also relates to coating of various physical systems. Motivation for the study of coating of both elastic and elastocapillary interfaces was discussed in our previous paper, Dixit & Homsy (2013): examples of their occurrence include particles and surfactants at interfaces, lipid bilayers, and elastic membranes. As also discussed in Dixit & Homsy (2013), the study of coating of elastic interfaces was motivated in part by experiments of Ouriemi & Homsy (2013) where the film thickness was obtained in a dip-coating flow by covering the interface by a monolayer of surface-adsorbed hydrophobic particles. The power law scaling, (1.2), is in qualitative agreement with that obtained in those experiments, which suggests that elasticity plays a role in particle-laden interfacial flows. However, for many of the relevant systems (particle-laden interfaces, surfactant films at high concentration, and lipid bilayers), the effect of surface tension is often not negligible, and so the combined effects of surface tension and elasticity must be taken into account, as in the present paper.

Elastocapillary effects arise in many natural systems. Bico *et al.* (2004) show that bundles of elastic lamellae clump together when dipped in a fluid as a result of a balance of capillary forces and elasticity of the lamellae. That study was carried out to understand why wet hair often clumps together. Kim & Mahadevan (2006) study the capillary rise of fluid between flexible sheets to determine the static equilibrium shapes. Duprat, Aristoff & Stone (2011) study the temporal dynamics of capillary rise between flexible sheets and show that elasticity of the sheet results in deviation from the classical diffusive-like behaviour. The role of elasticity of the substrate on

the shape and stability of sessile drops has been speculated about for a long time in connection with the relevance of Young's equation at the three-phase contact line. Das *et al.* (2011) calculate the deformation of an elastic substrate due to tangential capillary forces at the contact line. When a drop impacts on an elastic sheet, these contact line forces can deform the elastic sheet such that the drop can sometimes be wrapped around the sheet. By choosing elastic sheets of various shapes, Py *et al.* (2007) produce three-dimensional capillary origami structures. Finally, Pihler-Puzović *et al.* (2012) recently showed that replacing the rigid upper surface of a Hele-Shaw cell with an elastic membrane can suppress viscous fingering.

In all the problems described above, the resultant dynamics is a result of a complex interplay between surface tension and elasticity. In the present paper, we study elastocapillary effects in the classical Landau–Levich problem. Hence this paper is a natural extension of Dixit & Homsy (2013) to include elastocapillary effects. Our focus is on developing a general theory of elastocapillary Landau–Levich flow with the intention of uncovering the key physical mechanisms involved in determining the flow and the film thickness.

The paper is organized as follows. In §2, we introduce the relevant governing equations and dimensionless parameters. In §3, we obtain elastic corrections to the classical Landau–Levich problem in the limit when elasticity is weak relative to surface tension. When elasticity and surface tension are of comparable magnitude, we have the elastocapillary regime discussed in §4. The strong elasticity limit where surface tension is weak relative to elasticity is briefly discussed in §5. We summarize the paper in §6 and discuss open problems for future work.

2. Governing equations

Consider a vertical flat plate rising from a reservoir of fluid with a constant velocity, U, as shown schematically in figure 1(*a*). The density of the fluid is ρ and we neglect the effect of the surrounding air. The schematic of the flow field shows an elastocapillary interface possessing a combination of elasticity and surface tension. Away from the plate, the interface becomes flat at $x = 0$. The governing equations for the fluid below the interface in steady-state conditions can be written in dimensional form as

$$\nabla \cdot \tilde{\boldsymbol{u}} = 0, \qquad (2.1a)$$

$$\tilde{\boldsymbol{u}} \cdot \nabla \tilde{\boldsymbol{u}} = \frac{-1}{\rho} \nabla \tilde{p} + \frac{\mu}{\rho} \nabla^2 \tilde{\boldsymbol{u}} + g, \qquad (2.1b)$$

where $\tilde{\boldsymbol{u}}$ is the dimensional velocity, ρ is the density of the fluid, g is the acceleration due to gravity, μ is the dynamic viscosity and $\tilde{p}$ is the dimensional pressure. We model the elasticity of the interface using the Helfrich model,

$$E_C = \frac{1}{2} \int K_B (\tilde{\kappa} - \tilde{\kappa}_0)^2 \, \mathrm{d}A + \oint \gamma \, \mathrm{d}C, \qquad (2.2)$$

where E_C is the elastic energy, K_B is the bending modulus, and $\tilde{\kappa}$ and $\tilde{\kappa}_0$ are the dimensional mean and spontaneous curvatures respectively. In the first term, the integration is performed over the surface area of the interface and the second term describes the line tension term. Since the present study is restricted to two dimensions, the line tension term does not enter the analysis. For simplicity, we neglect the effect of spontaneous curvature, though this can easily be incorporated into the present analysis.
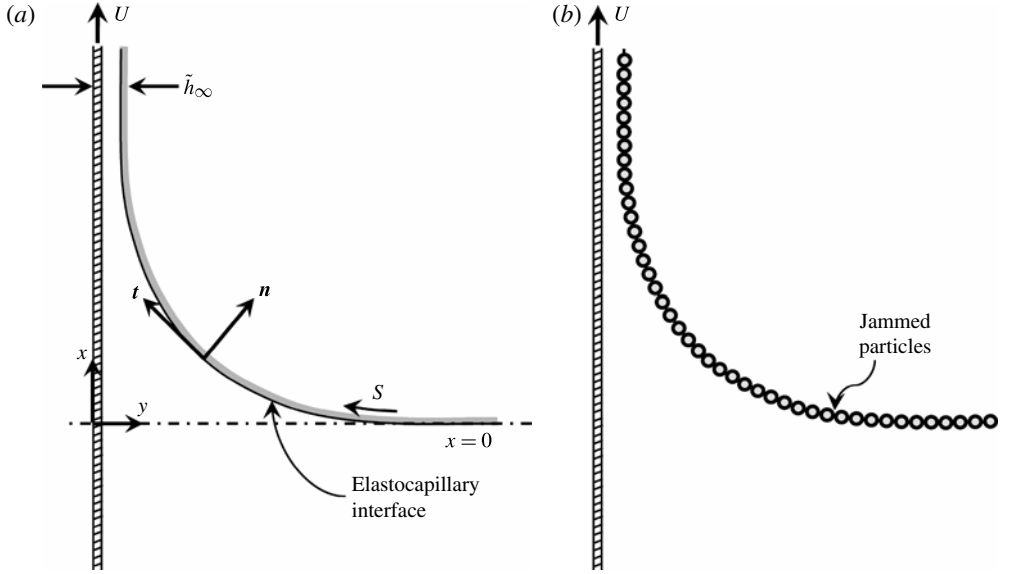
FIGURE 1. A schematic of the Landau–Levich dip-coating problem: (*a*) with an elastocapillary interface possessing both elasticity and surface tension, and (*b*) with a jammed monolayer of particles.

We introduce an additional energy contribution from surface tension which takes the usual form

$$E_T = \int \sigma \, dA, \tag{2.3}$$

where (we recall) σ is the surface tension of the interface. A similar term appears in the case of closed lipid membranes such as vesicles where σ is interpreted as a Lagrange multiplier providing an area constraint for an incompressible interface. In fact, in certain cases Seifert (1995) has shown that σ can indeed be interpreted as an effective tension. For a two-dimensional interface, the integration is performed along a line, and hence dA can be replaced by ds, where s is the arclength coordinate measured in the direction of the tangent.

Owing to the close similarities between elastic interfaces and particle-laden films (Vella, Aussillous & Mahadevan 2004), we can place the present study in the context of particle-laden Landau–Levich flows. In this case, we replace the elastic interface with a jammed monolayer of particles as shown in figure 1(*b*). From an experimental viewpoint, such a jammed monolayer is an idealization, since particle concentration will inevitably vary along the interface. Nevertheless, we expect such a model to closely resemble a saturated interface covered with particles, as was the case in the experiments of Ouriemi & Homsy (2013). In this case, γ represents line tension around 'islands' of particle clusters. If the size of the particles is small relative to the mean radius of curvature of the interface, it was shown by Planchette, Lorenceau & Biance (2012) that the spontaneous curvature is small. This is consistent with the neglect of $\tilde{\kappa}_0$ in the present analysis.

Given these approximations and using the procedure given in Kaoui *et al.* (2008), we derive expressions for the interfacial forces from (2.2) and (2.3), the result being

written as

$$f_C = -K_B \left(\frac{\partial^2 \tilde{\kappa}}{\partial s^2} + \frac{\tilde{\kappa}^3}{2} \right) n, \tag{2.4a}$$

$$f_T = \sigma \kappa n, \tag{2.4b}$$

where n is the unit vector in the normal direction and the subscripts C and T denote that the forces correspond to curvature-induced elastic force and surface tension force respectively. In deriving (2.4a) and (2.4b), we assume a constant K_B and σ along the interface. The normal and tangential stress balance equations on the interface at $y = h(x)$ take the form

$$n \cdot \tilde{T} \cdot n = -K_B \left(\frac{\partial^2 \tilde{\kappa}}{\partial s^2} + \frac{\tilde{\kappa}^3}{2} \right) + \sigma \tilde{\kappa}, \tag{2.5a}$$

$$t \cdot s\tilde{f}T \cdot n = 0, \tag{2.5b}$$

where t is the unit vector in the tangential direction and $\tilde{T} = -\tilde{p}I + \mu[\nabla \tilde{u} + \nabla \tilde{u}^{\mathrm{T}}]$ is the stress tensor. In writing these equations, the effect of interfacial viscosity is neglected. The boundary conditions on the plate and on the free surface are given by

$$\tilde{u} = \tilde{U} \quad \text{at } \tilde{y} = 0, \tag{2.6}$$

$$n \cdot \tilde{u} = 0 \quad \text{at } \tilde{y} = \tilde{h}(\tilde{x}). \tag{2.7}$$

As they are dimensionless, the tilde decoration is not used for the normal and tangential vectors. In terms of $\tilde{h}(\tilde{x})$, these vectors take the form

$$n = \frac{-\tilde{h}_{\tilde{x}} \hat{i} + \hat{j}}{(1 + \tilde{h}_{\tilde{x}}^2)^{1/2}}, \quad t = \frac{\hat{i} + \tilde{h}_{\tilde{x}} \hat{j}}{(1 + \tilde{h}_{\tilde{x}}^2)^{1/2}} \quad \text{with } \tilde{h}_{\tilde{x}} = \frac{\mathrm{d}\tilde{h}}{\mathrm{d}\tilde{x}}, \tag{2.8}$$

where $\hat{i}$ and $\hat{j}$ are the unit vectors in the x and y directions respectively. The dimensional curvature, $\tilde{\kappa}$ can be written as

$$\tilde{\kappa} = \frac{\tilde{h}_{\tilde{x}\tilde{x}}}{(1 + \tilde{h}_{\tilde{x}}^2)^{3/2}}. \tag{2.9}$$

2.1. *Non-dimensional numbers and regimes of interest*

To completely characterize the problem, we define the following non-dimensional numbers:

$$\text{Reynolds number, } Re = \frac{\rho U l_c}{\mu}, \tag{2.10a}$$

$$\text{capillary number, } Ca = \frac{\mu U}{\sigma}, \tag{2.10b}$$

$$\text{elasticity number, } El = \frac{\mu U l_e^2}{K_B}. \tag{2.10c}$$

It is convenient to define an elastocapillary number, $\epsilon = K_B / \sigma l_c^2$, which is independent of the plate speed and is related to Ca and El through the expression

$$\epsilon = \left(\frac{Ca}{El} \right)^2. \tag{2.11}$$

The theory developed in this paper is valid in the following limiting conditions:

$$Re \ll 1, \quad Ca \ll 1, \quad El \ll 1. \tag{2.12}$$

Based on the relative strengths of surface tension and elasticity, various flow regimes are possible defined based on the size of ϵ as follows:

(*a*) $\epsilon \ll 1$: weak elasticity regime;
(*b*) $\epsilon \sim O(1)$: elastocapillary regime;
(*c*) $\epsilon \gg 1$: strong elasticity regime.

As the name suggests, in the weak elasticity regime, surface tension dominates over elasticity. Hence the natural length scale in this regime is the capillary length, l_c. The resulting solution will be a small correction (in an asymptotic sense) to the classical Landau–Levich flow. We develop such a solution in § 3. In the strong elasticity regime, surface tension is weak relative to elasticity. Hence the natural length scale in this regime is the elasticity length, l_e. The resulting solution will be a small correction to the elastic Landau–Levich flow studied in Dixit & Homsy (2013) and discussed in § 5. And finally, in the elastocapillary regime discussed in § 4, both elasticity and surface tension are of comparable magnitude. In this case, it will be convenient to introduce a new length scale, the elastocapillary length, which involves a balance of elasticity and surface tension.

3. Weak elasticity regime

We first investigate the effect of weak elasticity on the classical Landau–Levich flow. Our main interest is to calculate the departure of the film thickness from the classical case. As in the classical case, the domain is divided into three regions as shown in figure 2: a constant film region, a static region and an all-important transition region connecting them as discussed in Park & Homsy (1984).

3.1. *Non-dimensional equations: static region*

Since surface tension effects dominate over elasticity, we scale all lengths by the capillary length, l_c, velocities by plate speed U and pressure by σ/l_c. The governing equations in non-dimensional form are given by

$$u_x + v_y = 0, \tag{3.1a}$$

$$Ca\,Re(uu_x + vu_y) = -p_x + Ca\nabla^2 u - 1, \tag{3.1b}$$

$$Ca\,Re(uv_x + vv_y) = -p_y + Ca\nabla^2 v, \tag{3.1c}$$

$$u = 1, \quad v = 0 \quad \text{at } y = 0. \tag{3.2}$$

At $y = h(x)$, we have

$$v - h_x u = 0, \tag{3.3a}$$

$$
\begin{aligned}
-p + \frac{2Ca}{(1+h_x^2)}\left\{u_x(h_x^2 - 1) - (u_y + v_x)h_x\right\} &= \frac{h_{xx}}{(1+h_x^2)^{3/2}} \\
&\quad - \epsilon\left[\frac{2(1+h_x^2)^2 h_{xxxx} - 20(1+h_x^2)h_x h_{xx} h_{xxx} - 5(1-6h_x^2)h_{xx}^3}{2(1+h_x^2)^{9/2}}\right],
\end{aligned} \tag{3.3b}
$$

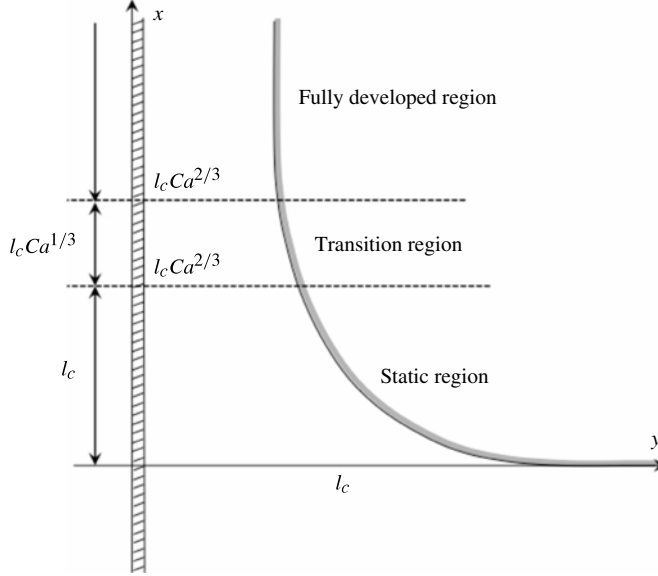$$-4u_x h_x + (u_y + v_x)(1 - h_x^2) = 0. \tag{3.3c}$$

FIGURE 2. The asymptotic structure of the flow in the weak elasticity regime showing the breakdown of the region into three regions: (i) a static region where gravity balances surface tension; (ii) a transition region where viscous stress balances surface tension; and (iii) a fully developed region where the flow is uniform.

As can be seen from (3.1*b*), (3.1*c*) and (3.3*b*), the viscous normal stress is negligible for small *Ca*. The field equations show that the pressure is constant and all flow effects are of higher order. The normal stress balance shows that this pressure is balanced by a combination of surface tension and elasticity. Solutions in this region cannot match the uniform flow region, so we rescale all variables as shown below.

3.2. *Non-dimensional equations: transition region*

In the transition region, all the variables are rescaled according to the scalings given in Bretherton (1961) and Park & Homsy (1984). All the inner variables are shown with an overbar. In this region, viscous forces become as important as the pressure or interfacial tension and the equation of motion is given by the lubrication approximation. The relevant scalings in this region are (see Park & Homsy 1984 for more details)

$$(\bar{x}, \bar{y}) = \left(\frac{x - l}{Ca^{1/3}}, \frac{y}{Ca^{2/3}} \right), \tag{3.4a}$$

$$(\bar{u}, \bar{v}) = \left(u, \frac{v}{Ca^{1/3}} \right), \tag{3.4b}$$

$$\bar{p} = p, \quad \bar{h} = \frac{h}{Ca^{2/3}}. \tag{3.4c}$$

The non-dimensional equations in the transition region in terms of rescaled variables become

$$\bar{u}_{\bar{x}} + \bar{v}_{\bar{y}} = 0, \tag{3.5a}$$

$$Ca\, Re(\bar{u}\bar{u}_{\bar{x}} + \bar{v}\bar{u}_{\bar{y}}) = -\bar{p}_{\bar{x}} + Ca^{2/3}\bar{u}_{\bar{x}\bar{x}} + \bar{u}_{\bar{y}\bar{y}} - Ca^{1/3}, \tag{3.5b}$$

$$Ca\,Re(\bar{u}\bar{v}_{\bar{x}} + \bar{v}\bar{v}_{\bar{y}}) = -\bar{p}_{\bar{y}} + Ca^{4/3}\bar{v}_{\bar{x}\bar{x}} + Ca^{2/3}\bar{v}_{\bar{y}\bar{y}}, \qquad (3.5c)$$

$$\bar{u} = 1, \quad \bar{v} = 0 \quad \text{at } \bar{y} = 0. \qquad (3.6)$$

At $\bar{y} = \bar{h}(\bar{x})$, we have

$$\bar{v} - \bar{h}_{\bar{x}}\bar{u} = 0, \qquad (3.7a)$$

$$-\bar{p} + \frac{2Ca^{2/3}}{(1 + Ca^{2/3}\bar{h}_{\bar{x}}^2)}\left[-\bar{h}_{\bar{x}}(\bar{u}_{\bar{y}} + Ca^{2/3}\bar{v}_{\bar{x}}) - \bar{u}_{\bar{x}} + Ca^{2/3}\bar{u}_{\bar{x}}\bar{h}_{\bar{x}}^2\right]$$
$$= \frac{\bar{h}_{\bar{x}\bar{x}}}{(1 + Ca^{2/3}\bar{h}_{\bar{x}}^2)^{3/2}} - \frac{\epsilon}{(1 + Ca^{2/3}\bar{h}_{\bar{x}}^2)^{9/2}}\left[\frac{1}{Ca^{2/3}}\bar{h}_{\bar{x}\bar{x}\bar{x}\bar{x}} + O(1)\right], \qquad (3.7b)$$

$$-4Ca^{2/3}\bar{u}_{\bar{x}}\bar{h}_{\bar{x}} + (\bar{u}_{\bar{y}} + Ca^{2/3}\bar{v}_{\bar{x}})(1 - Ca^{2/3}\bar{h}_{\bar{x}}^2) = 0. \qquad (3.7c)$$

For brevity, only the dominant elastic term is written in the normal stress balance.

3.3. *Asymptotic expansion*

The nature of the scaling in the transition region suggests that all unknown quantities may be expanded in simple powers of Ca as follows:

$$h(x; Ca, \epsilon) = \sum_{j=0}^{\infty} Ca^{j/3}h^j(x; \epsilon), \qquad (3.8a)$$

$$p(x, y; Ca, \epsilon) = \sum_{j=0}^{\infty} Ca^{j/3}p^j(x, y; \epsilon), \qquad (3.8b)$$

$$\boldsymbol{u}(x, y; Ca, \epsilon) = \sum_{j=0}^{\infty} Ca^{j/3}\boldsymbol{u}^j(x, y; \epsilon). \qquad (3.8c)$$

For simplicity, we only evaluate the leading-order terms in the expansion. The size of ϵ is undetermined at this point and is therefore carried forward in the analysis.

3.4. *Static region: leading order*

On substituting (3.8) into (3.1)–(3.3), the governing equations in the static region at leading order become

$$u_x^0 + v_y^0 = 0, \qquad (3.9a)$$
$$p_x^0 = -1, \qquad (3.9b)$$
$$p_y^0 = 0, \qquad (3.9c)$$

$$u^0 = 1, \quad v^0 = 0 \quad \text{at } y = 0. \qquad (3.10)$$

At $y = h^0(x)$, we have

$$u^0 h_x^0 - v^0 = 0, \qquad (3.11a)$$

$$p^0 + \frac{h_{xx}^0}{(1 + (h_x^0)^2)^{3/2}}$$
$$- \epsilon\left[\frac{2(1 + (h_x^0)^2)^2 h_{xxxx}^0 - 20(1 + (h_x^0)^2)h_x^0 h_{xx}^0 h_{xxx}^0 - 5(1 - 6(h_x^0)^2)(h_{xx}^0)^3}{2(1 + (h_x^0)^2)^{9/2}}\right] = 0. \qquad (3.11b)$$

In the absence of elasticity, the normal stress balance equation at leading order reduces to the Young–Laplace equation. In such a case, the static region is commonly referred to as the capillary-statics region. In the present case however, elasticity also determines the interface shape. The interface far away from the plate has to be nearly flat and is determined by the balance of hydrostatic pressure, surface tension and elasticity. The boundary conditions for the interface shape are given by

$$h^0 \to \infty \quad \text{as } x \to 0, \tag{3.12a}$$

$$h_x^0 \to -\infty \quad \text{as } x \to 0. \tag{3.12b}$$

As is well known, boundary conditions on the plate for the static meniscus are determined by matching this region to the transition region.

3.5. *Transition region: leading order*

On substituting (3.8) into (3.5)–(3.7), the governing equations in the transition region at leading order become

$$\bar{u}_{\bar{x}}^0 + \bar{v}_{\bar{y}}^0 = 0, \tag{3.13a}$$

$$\bar{p}_{\bar{x}}^0 = \bar{u}_{\bar{y}\bar{y}}^0, \tag{3.13b}$$

$$\bar{p}_{\bar{y}}^0 = 0, \tag{3.13c}$$

$$\bar{u}^0 = 1, \quad \bar{v}^0 = 0 \quad \text{at } \bar{y} = 0. \tag{3.14}$$

At $\bar{y} = \bar{h}^0(\bar{x})$, we have

$$\bar{u}^0 \bar{h}_{\bar{x}}^0 - \bar{v}^0 = 0, \tag{3.15a}$$

$$\bar{p}^0 + \bar{h}_{\bar{x}\bar{x}}^0 - \frac{\epsilon}{Ca^{2/3}} \bar{h}_{\bar{x}\bar{x}\bar{x}\bar{x}}^0 = 0, \tag{3.15b}$$

$$\bar{u}_{\bar{y}}^0 = 0. \tag{3.15c}$$

To proceed further, we need to know the magnitude of ϵ relative to $Ca^{2/3}$. Observe that in the transition region, ϵ only appears in the ratio $\epsilon/Ca^{2/3}$. We therefore define a new parameter

$$\mathscr{E} = \frac{\epsilon}{Ca^{2/3}}, \tag{3.16}$$

which is assumed to be small. We wish to ensure that the first correction to the classical Landau–Levich problem is due to elasticity. Since Wilson (1982) showed that gravity becomes important at $O(Ca^{1/3})$, we impose the following bounds on the magnitude of $\mathscr{E}$:

$$Ca^{1/3} \ll \mathscr{E} \ll 1. \tag{3.17}$$

We assume that all variables in (3.9)–(3.15) may be expanded in powers of $\mathscr{E}$ as follows:

$$[h^0(x; \mathscr{E}), \bar{h}^0(\bar{x}; \mathscr{E})] = \sum_{i=0}^{\infty} \mathscr{E}^i [h^{i0}(x), \bar{h}^{i0}(\bar{x})], \tag{3.18a}$$

$$[p^0(x; \mathscr{E}), \bar{p}^0(\bar{x}; \mathscr{E})] = \sum_{i=0}^{\infty} \mathscr{E}^i [p^{i0}(x), \bar{p}^{i0}(\bar{x})], \tag{3.18b}$$

$$[\boldsymbol{u}^0(x, y; \mathscr{E}), \bar{\boldsymbol{u}}^0(\bar{x}, \bar{y}; \mathscr{E})] = \sum_{i=0}^{\infty} \mathscr{E}^i [\boldsymbol{u}^{i0}(x, y), \bar{\boldsymbol{u}}^{i0}(\bar{x}, \bar{y})]. \tag{3.18c}$$

Though the above expansions are written to all orders in $\mathscr{E}$, owing to the restriction imposed in (3.17) the sequential ordering of terms in (3.18) will break down beyond linear terms in $\mathscr{E}$. We therefore only obtain solutions up to $O(\mathscr{E})$ in the following sections.

3.6. $O(\mathscr{E}^0 Ca^0)$ solutions

The leading-order problem in $\mathscr{E}$ and Ca is the well-known Landau–Levich problem without any elastic effects. We follow the solution procedure outlined in Park & Homsy (1984) and briefly repeat the analysis here to establish the solution procedure for higher-order elastic corrections. We substitute (3.18) in (3.9)–(3.15) and obtain the leading-order equations in both $\mathscr{E}$ and Ca. From (3.11b), the leading-order normal stress balance equation takes the form

$$p^{00} + \frac{h_{xx}^{00}}{(1 + (h_x^{00})^2)^{3/2}} = 0. \tag{3.19}$$

Eliminating p^{00} using (3.9b) and using boundary conditions (3.12), the interface shape takes the form (see Park 1991)

$$h^{00}(x) = \operatorname{sech}^{-1}\left(\frac{x}{2}\right) - (4 - x^2)^{1/2} + C, \tag{3.20}$$

where C is the integration constant determined by matching this solution to the transition region. The normal stress balance in the transition region at leading order becomes

$$\bar{p}^{00} + \bar{h}_{\bar{x}\bar{x}}^{00} = 0. \tag{3.21}$$

We now integrate the momentum equation (3.13b) with appropriate boundary conditions on the plate and the interface to obtain $\bar{u}^{00}$ in terms of pressure gradient, $\bar{p}_{\bar{x}}^{00}$. This, together with the normal stress balance (3.21) and conservation of mass, leads to a simple differential equation for the film thickness, $\bar{h}^{00}(\bar{x})$,

$$\bar{h}_{\bar{x}\bar{x}\bar{x}}^{00} = \frac{3(\bar{h}_\infty^{00} - \bar{h}^{00})}{(\bar{h}^{00})^3}. \tag{3.22}$$

This is the well-known Landau–Levich equation with $\bar{h}_\infty^{00}$ being the leading-order fully developed film thickness (see Park & Homsy 1984 for more details). Far away from the plate, the solution of this equation assumes a simple quadratic form

$$\bar{h}^{00} = C_0 \bar{x}^2 + C_1 \bar{x} + C_2 \quad \text{as } \bar{x} \to -\infty. \tag{3.23}$$

The unknowns C_0, C_1 and C_2 are determined by matching conditions.

To complete the leading-order analysis, the solution in the transition region has to be matched with the static region. The matching condition can be written as

$$\lim_{\bar{x} \to -\infty} Ca^{2/3} \bar{h}(\bar{x}) = \lim_{x \to l} h(x). \tag{3.24}$$

Expanding l in $\mathscr{E}$, the matching conditions for h^{00} become

$$O(\mathscr{E}^0 Ca^0): \quad h^{00}(l^0) = 0, \tag{3.25a}$$

$$O(\mathscr{E}^0 Ca^{1/3}): \quad h_x^{00}(l^0) = 0, \tag{3.25b}$$

$$O(\mathscr{E}^0 Ca^{2/3}): \quad h_{xx}^{00}(l^0) = 2C_0. \tag{3.25c}$$

From the first two conditions, the constant C in (3.20) is found and the value of l^0 is found to be $\sqrt{2}$. Using these results, the interface shape in the static region takes the form

$$h^{00}(x) = \text{sech}^{-1}\left(\frac{x}{2}\right) - (4 - x^2)^{1/2} - \text{sech}^{-1}\left(\frac{1}{\sqrt{2}}\right) + \sqrt{2}. \tag{3.26}$$

From the last condition in (3.25), we obtain the curvature of the interface at $x = l^0$ to be $\sqrt{2}$ and therefore the constant $C_0 = 1/\sqrt{2}$. The film thickness, $\bar{h}_\infty^{00}$, in (3.22) is the value at which the far-field asymptotic behaviour is consistent with the quadratic expression (3.23). The numerical integration of (3.22) is similar to that carried out in Park & Homsy (1984) and Park (1991) and results in a non-dimensional film thickness of 0.9458. Therefore, the film thickness at leading order in $\mathscr{E}$ and Ca is given by

$$h_\infty^{00} = 0.9458 Ca^{2/3}. \tag{3.27}$$

This is the famous Landau–Levich law.

3.7. $O(\mathscr{E} Ca^0)$ equations

We now obtain the first elastic correction to the Landau–Levich flow. The elastic correction to the normal stress balance equation in the static region becomes

$$p^{10} + \frac{h_{xx}^{10}}{\left(1 + (h_x^{00})^2\right)^{3/2}} - \frac{3 h_x^{10} h_x^{00} h_{xx}^{00}}{\left(1 + (h_x^{00})^2\right)^{5/2}} = 0. \tag{3.28}$$

Viscous effects become important only at $O(Ca^{2/3})$; therefore the normal stress balance is the only relevant condition in the static region.

The first elastic correction to the normal stress balance in the transition region becomes

$$\bar{p}^{10} + \bar{h}_{\bar{x}\bar{x}}^{10} - \bar{h}_{\bar{x}\bar{x}\bar{x}\bar{x}}^{00} = 0. \tag{3.29}$$

Solving for the velocity field from the momentum equations, a linear third-order differential equation for $\bar{h}^{10}(\bar{x})$ can be easily obtained:

$$\bar{h}_{\bar{x}\bar{x}\bar{x}}^{10} = \frac{3\left[\bar{h}^{10}(2\bar{h}^{00} - 3\bar{h}_\infty^{00}) + \bar{h}^{00}\bar{h}_\infty^{10}\right]}{(\bar{h}^{00})^4} + \bar{h}_{\bar{x}\bar{x}\bar{x}\bar{x}\bar{x}}^{00}, \tag{3.30}$$

where $\bar{h}_\infty^{10}$ is the first elastic correction to the thickness of the fully developed thin film. Equation (3.30) can be transformed into a canonical form using the following transformation:

$$\eta^{10} = \frac{\bar{h}^{10}}{\bar{h}_\infty^{00}}, \quad \xi = \frac{\bar{x} + t}{\bar{h}_\infty^{00}}, \quad R = \frac{\bar{h}_\infty^{10}}{\bar{h}_\infty^{00}}, \quad \eta^{00} = \frac{\bar{h}^{00}}{\bar{h}_\infty^{00}}. \tag{3.31}$$

Equation (3.30) then becomes

$$\eta_{\xi\xi\xi}^{10} = \frac{3\left[\eta^{10}(2\eta^{00} - 3) + R\eta^{00}\right]}{(\eta^{00})^4} + \frac{1}{(\bar{h}_\infty^{00})^2}\eta_{\xi\xi\xi\xi\xi}^{00}, \tag{3.32}$$

with boundary condition

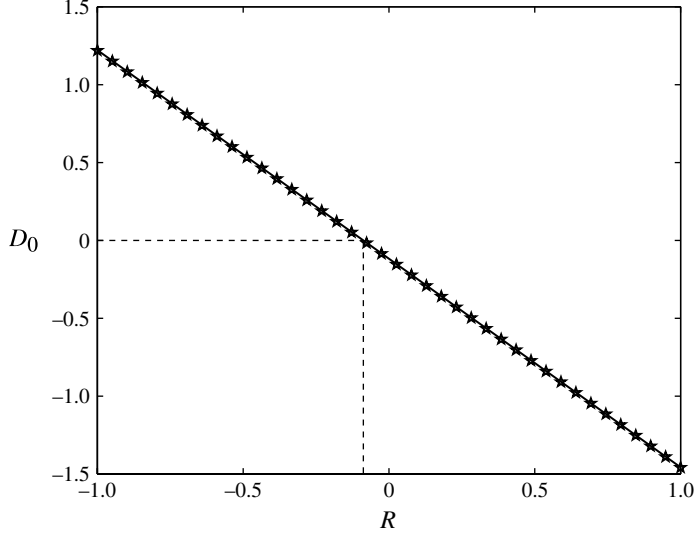$$\eta^{10} \to R \quad \text{as } \xi \to \infty. \tag{3.33}$$

FIGURE 3. A schematic of the Landau–Levich dip-coating problem in the absence of any impurities showing the presence of an interfacial stagnation point.

As $\xi \to -\infty$, η^{10} assumes a simple quadratic form:

$$\eta^{10}(\xi) = \tfrac{1}{2}D_0\xi^2 + D_1\xi + D_2, \tag{3.34}$$

or, in terms of original scaling, we get

$$\bar{h}^{10}(\bar{x}) = \frac{D_0}{2\bar{h}_\infty^{00}}\bar{x}^2 + \left(\frac{D_0 t}{\bar{h}_\infty^{00}} + D_1\right)\bar{x} + \left(\frac{D_0 t^2}{2\bar{h}_\infty^{00}} + D_1 t + D_2\bar{h}_\infty^{00}\right). \tag{3.35}$$

The matching conditions for h^{10} at $O(\mathscr{E})$ become

$$O(\mathscr{E}Ca^0): \quad h^{10}(l^0) = 0, \tag{3.36a}$$

$$O(\mathscr{E}Ca^{1/3}): \quad h_x^{10}(l^0) = 0, \tag{3.36b}$$

$$O(\mathscr{E}Ca^{2/3}): \quad h_{xx}^{10}(l^0) = \frac{D_0}{\bar{h}_\infty^{00}}. \tag{3.36c}$$

From the solution of (3.28), it can be shown that $h_{xx}^{10}(l^0) = 0$, therefore D_0 must be zero. By numerical integration of (3.32) for various R, we determine the value of R for which D_0 vanishes, as shown in figure 3. From a straight line fit to the solution, we find

$$R = -0.0879 \pm 0.01 \quad \text{at } D_0 = 0. \tag{3.37}$$

By varying the domain size and the allowable tolerance in the numerical integration, the value of R slightly varied as reflected in the error bar. The negative value for R shows that the first elastic correction to the Landau–Levich flow results in film thinning in the weak elasticity regime. The modified Landau–Levich law in this regime becomes

$$h_\infty = (0.9458 - 0.0839\mathscr{E})Ca^{2/3}. \tag{3.38}$$

In this section, we considered the limiting case where $\epsilon \ll Ca^{2/3}$. A natural extension of this section would be the case where $\epsilon \sim O(Ca^{2/3})$. A valid solution in this region of parameter space could not be found; see Appendix for further details.

4. Elastocapillary regime

4.1. *Scaling and static region*

We now consider the case when elasticity and surface tension effects are comparable to each other. It is therefore natural to define a length scale based on the balance of elasticity and surface tension. In the outer region where viscous stresses are negligible, we have $p \sim K_B h_{xxxx} \sim \sigma h_{xx}$. Assuming x and h scale with the length scale L, we get

$$\frac{K_B}{L^3} \sim \frac{\sigma}{L} \Rightarrow L = \left(\frac{K_B}{\sigma} \right)^{1/2}, \tag{4.1}$$

where L can be called an elastocapillary length. This length scale was also used in Kim & Mahadevan (2006). Using L as the characteristic length scale, the full momentum equations and boundary conditions simplify considerably. The only relevant equations in the static region are the hydrostatic equation and the normal stress balance,

$$p_x = -\epsilon, \tag{4.2a}$$

$$p = \frac{-h_{xx}}{(1+h_x^2)^{3/2}} + \left[\frac{2(1+h_x^2)^2 h_{xxxx} - 20(1+h_x^2)h_x h_{xx} h_{xxx} - 5(1-6h_x^2)h_{xx}^3}{2(1+h_x^2)^{9/2}} \right]. \tag{4.2b}$$

In the above equations, the viscous normal stress terms have been omitted as they are negligible in the static region. It is useful to note that the parameter

$$\epsilon = \frac{L^2}{l_c^2} = \frac{K_B \rho g}{\sigma^2}. \tag{4.3}$$

This relation will be useful in rescaling the results obtained in this section in terms of l_c and l_e for comparison with the weak and strong elasticity regimes respectively.

4.2. *Transition region*

As before, the solution of the static equations cannot be matched to the fully developed thin-film solution near the plate. We again introduce a transition region where viscous forces become important and also invoke the lubrication approximation. To determine the relevant scalings in this region (shown with an overbar), we introduce a general rescaling of both the x and y coordinates:

$$(\bar{x}, \bar{y}) = \left(\frac{x}{Ca^n}, \frac{y}{Ca^m} \right), \quad \bar{h} = \frac{h}{Ca^m}, \quad \bar{p} = p, \quad (\bar{u}, \bar{v}) = \left(u, \frac{v}{Ca^{m-n}} \right). \tag{4.4}$$

Again, the full momentum equations and boundary conditions simplify, with the relevant ones being the x-momentum equation, the continuity equation and the normal stress balance. Writing the *dominant terms* in the x-momentum equation, (3.1b), and the normal stress balance equation, (3.3b), we get

$$\bar{p}_{\bar{x}} = Ca^{1+n-2m}\bar{u}_{\bar{y}\bar{y}} - \epsilon Ca^n, \tag{4.5a}$$

$$-\bar{p} = Ca^{m-2n}\bar{h}_{\bar{x}\bar{x}} + Ca^{m-4n}\bar{h}_{\bar{x}\bar{x}\bar{x}\bar{x}}. \tag{4.5b}$$

The first relation refers to the balance of pressure gradient with viscous stress and gravity and the second relation refers to the balance of pressure with surface tension and elasticity. We require that these terms balance as $Ca \to 0$. From (4.5), we have two options:

$$n = 2m - 1, \quad m - 2n = 0, \tag{4.6a}$$

$$\text{or} \quad n = 2m - 1, \quad m - 4n = 0. \tag{4.6b}$$

Using the first set of relations in (4.6a), we get $n = 1/3$ and $m = 2/3$ (note that this gives the classical Landau–Levich scaling). With this scaling, the elasticity term in (4.5b) is $O(Ca^{-2/3})$ which cannot be balanced in the limit $Ca \to 0$. The second set of relations in (4.6b) yield $n = 1/7$ and $m = 4/7$, with the surface tension term in (4.5) now being $O(Ca^{2/7})$ and therefore small at leading order. Hence the only meaningful transition region scalings are obtained with $m = 4n = 4/7$. The rescaled variables in the transition region are therefore

$$(\bar{x}, \bar{y}) = \left(\frac{x - x_0}{Ca^{1/7}}, \frac{y}{Ca^{4/7}} \right), \tag{4.7a}$$

$$(\bar{u}, \bar{v}) = \left(u, \frac{v}{Ca^{3/7}} \right), \tag{4.7b}$$

$$\bar{p} = p, \quad \bar{h} = \frac{h}{Ca^{4/7}}. \tag{4.7c}$$

Now the leading-order normal stress balance equation in the transition region becomes

$$\bar{p} = \bar{h}_{\bar{x}\bar{x}\bar{x}\bar{x}}. \tag{4.8}$$

Solving for the velocity field from the momentum equation and conserving mass flux, we get

$$\bar{h}_{\bar{x}\bar{x}\bar{x}\bar{x}\bar{x}} = \frac{3(\bar{h} - \bar{h}_\infty)}{\bar{h}^3}. \tag{4.9}$$

Equation (4.9) is identical to the elastic Landau–Levich equation derived in Dixit & Homsy (2013) where surface tension was neglected. Thus surface tension contributes to the static region in the elastocapillary problem, but not to the inner transition region at leading order. Thus the development of the inner solution has a lot in common with our previous paper, Dixit & Homsy (2013), but we repeat certain details here for completeness.

As $\bar{x} \to \infty$, the solution of (4.9) has to match with a thin film of thickness $\bar{h}_\infty$. After linearizing it about $\bar{h} = \bar{h}_\infty$, we get

$$\bar{h}^{(0)} = \bar{h}_\infty^{(0)} + e^{\lambda_r \bar{x}} \{ A \cos(\lambda_i \bar{x}) + B \sin(\lambda_i \bar{x}) \} \quad \text{as } \bar{x} \to \infty, \tag{4.10}$$

where

$$\lambda_r + i\lambda_i = \frac{3^{1/5}}{\bar{h}_\infty^{3/5}} \left[\cos\left(\frac{4\pi}{5} \right) + i \sin\left(\frac{4\pi}{5} \right) \right], \tag{4.11}$$

and A, B are arbitrary constants. The constant B can be absorbed by making an arbitrary choice of the origin.

As the other end of the transition region, the film thickness diverges as $\bar{x} \to -\infty$ as shown in figure 1(a). Therefore the far-field asymptotic behaviour of $\bar{h}$ becomes

$$\bar{h}^{(0)} = c_0 \bar{x}^4 + c_1 \bar{x}^3 + c_2 \bar{x}^2 + c_3 \bar{x} + c_4 \quad \text{as } \bar{x} \to -\infty. \tag{4.12}$$

The constants c_i are unknown at this stage and have to be determined by matching with the static region.

In spite of the absence of surface tension in (4.9), surface tension affects the film thickness via the matching of the solution of (4.9) to the static meniscus as described below.

4.3. *Matching conditions*

According to the scaling (4.7), the film thickness in the transition region scales as $Ca^{4/7}$ times the thickness in the static region. Matching the two regions according to the matching principle of Van Dyke (1975), we get

$$\lim_{\bar{x} \to -\infty} Ca^{4/7} \bar{h}(\bar{x}) = \lim_{x \to x_0} h(x). \tag{4.13}$$

By using a Taylor series expansion of $h(x)$ about $x = x_0$, the matching conditions for $h^{(0)}$ and $h^{(1)}$ become

$$O(Ca^{(0)}): \quad h^{(0)}(x_0) = 0, \tag{4.14}$$

$$O(Ca^{1/7}): \quad h^{(0)}_x(x_0) = 0, \tag{4.15a}$$

$$h^{(1)}(x_0) = 0, \tag{4.15b}$$

$$O(Ca^{2/7}): \quad h^{(0)}_{xx}(x_0) = 0, \tag{4.16a}$$

$$h^{(1)}_x(x_0) = 0, \tag{4.16b}$$

$$O(Ca^{3/7}): \quad h^{(0)}_{xxx}(x_0) = 0, \tag{4.17a}$$

$$h^{(1)}_{xx}(x_0) = 0, \tag{4.17b}$$

$$O(Ca^{4/7}): \quad h^{(0)}_{xxxx}(x_0) = 24c_0, \tag{4.18a}$$

$$h^{(1)}_{xxx}(x_0) = 6c_1. \tag{4.18b}$$

The matching condition (4.14) clearly shows that x_0 is the position of contact of the static interface with the vertical plate. The matching conditions on $h^{(0)}$ serve as boundary conditions for the static interface shape governed by (4.2), as described in the next subsection.

4.4. *Static interface shape*

The detailed solution procedure for the static interface is outlined in Dixit & Homsy (2013). We therefore discuss only the key distinguishing feature pertinent to the present problem.

We first obtain the shape of the static interface far from the plate. In this region, elasticity balances gravity and the interface shape is governed by (3.11*b*). Since the boundary conditions are inhomogeneous as $x \to 0$, it is difficult to solve the static equations in the current coordinate system. Instead, we switch the coordinate system by assuming a one-to-one map from the (x, h) plane to the (η, ξ) plane as shown schematically in figure 4. In other words, we seek the solution of the static meniscus η as a function of ξ rather than h as a function of x. Eliminating pressure, the static equation for the interface height, $\eta = \eta(\xi)$, in the switched coordinate axes becomes

$$\eta_{\xi\xi\xi\xi} = -\epsilon\eta(1 + \eta_\xi^2)^{5/2} + (1 + \eta_\xi^2)\eta_{\xi\xi} + \frac{10\eta_\xi\eta_{\xi\xi}\eta_{\xi\xi\xi}}{(1 + \eta_\xi^2)} + \frac{5(1 - 6\eta_\xi^2)\eta_{\xi\xi}^3}{2(1 + \eta_\xi^2)^2}, \tag{4.19}$$
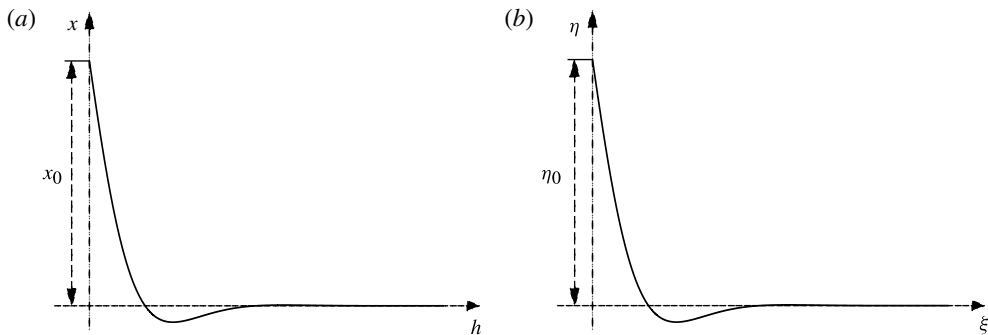
FIGURE 4. Transformation from the original (x, h) axes to (η, ξ) axes.

with $\eta \to 0$ as $\xi \to \infty$. Expanding η in powers of $Ca^{1/7}$ as

$$\eta = \eta^{(0)} + Ca^{1/7}\eta^{(1)} + O(Ca^{2/7}), \tag{4.20}$$

we obtain the leading-order solution and the first-order correction to the static interface as described below.

4.5. *The $O(1)$ static solution*

The equation for the leading-order term $\eta^{(0)}$ is identical to (4.19). After linearizing this equation about $\eta^{(0)} = 0$, we obtain the following characteristic equation for the eigenvalues λ:

$$\lambda^4 - \lambda^2 + \epsilon = 0. \tag{4.21}$$

Of the four roots, only two are physically relevant, and they take the form

$$\lambda_{1,2} = -\left(\frac{1 \pm \sqrt{1 - 4\epsilon}}{2}\right)^{1/2}. \tag{4.22}$$

For $\epsilon \leqslant 1/4$, the solution of (4.19) exhibits an exponential decay with no oscillations, while for $\epsilon > 1/4$, the eigenvalues assume complex values and the solution exhibits an oscillatory decay. The far-field behaviour then becomes

$$\eta^{(0)} = a e^{\lambda_1 \xi} + b e^{\lambda_2 \xi}. \tag{4.23}$$

We can eliminate the two constants a and b to obtain consistency conditions,

$$\left.\begin{aligned} \eta^{(0)}_{\xi\xi} &= (\lambda_1 + \lambda_2)\eta^{(0)}_\xi - \lambda_1\lambda_2\eta^{(0)} \\ \eta^{(0)}_{\xi\xi\xi} &= (\lambda_1 + \lambda_2)\eta^{(0)}_{\xi\xi} - \lambda_1\lambda_2\eta^{(0)}_\xi \end{aligned}\right\} \quad \text{as } \xi \to \infty. \tag{4.24}$$

We now examine the region close to the plate to obtain additional boundary conditions. Since $h_{xxxx} = 24c_0$ and all lower derivatives vanish at $x = x_0$ as shown in (4.14)–(4.18), the local interface shape near $x = x_0$ can be written as

$$h^{(0)} = c_0(x - x_0)^4 \quad \text{near } x = x_0. \tag{4.25}$$

Writing the above equation in terms of $(\xi, \eta^{(0)})$, we get

$$\xi = c_0(\eta^{(0)} - \eta_0)^4. \tag{4.26}$$

Rewriting the above result as an equation for $\eta^{(0)}$, we get

$$\eta^{(0)} = \eta_0 + d\xi^{1/4}, \tag{4.27a}$$

$$\eta_\xi^{(0)} = \frac{d}{4}\xi^{-3/4}, \tag{4.27b}$$

$$\eta_{\xi\xi}^{(0)} = -\frac{3d}{16}\xi^{-7/4}, \tag{4.27c}$$

$$\eta_{\xi\xi\xi}^{(0)} = \frac{21d}{64}\xi^{-11/4}, \tag{4.27d}$$

$$\eta_{\xi\xi\xi\xi}^{(0)} = -\frac{231d}{256}\xi^{-15/4}, \tag{4.27e}$$

where $d = c_0^{-1/4}$. The above expressions are consistent with the singular nature of the boundary conditions as $\xi \to 0$. For numerical purposes, the singular boundary conditions at $\xi = 0$ are applied at $\xi = 10^{-6}$. Substituting (4.27) into (4.19) and balancing the dominant terms as $\xi \to 0$, we get the simple result

$$\eta_0 = \frac{24}{\epsilon d^4}. \tag{4.28}$$

With two boundary conditions from (4.24) and three from (4.27), the formulation of the static problem for $\eta^{(0)}$ is now complete.

The solution procedure is similar to that discussed in Dixit & Homsy (2013). Since ϵ is a free parameter, we vary it in the range $[10^{-3}, 10^3]$. It has to be noted that for small values of ϵ, the decay rate can be very small. For example, using $\epsilon = 10^{-3}$, we get $\lambda_1 = -0.0316$ and $\lambda_2 = -0.9995$. Since $e^{\lambda_1\xi}$ decays slowly as $\xi \to \infty$, the domain of integration has to be considerably increased for small ϵ. For large ϵ, the domain of integration is $\xi \in [0, 20]$ and for small ϵ, we use $[0, 400]$.

The position of the apparent contact line η_0 or x_0 is shown in figure 5(*a*) which exhibits a power-law behaviour for both large and small ϵ. As a result, we closely examine the limiting cases $\epsilon \to 0$ and $\epsilon \to \infty$. Since ϵ is the ratio of elasticity to surface tension, $\epsilon \to 0$ corresponds to the limit of vanishing elasticity, and $\epsilon \to \infty$ corresponds to the limit of vanishing surface tension.

In the limit $\epsilon \to 0$, we expect the power law in figure 5(*a*) to approach $\eta_0 \sim \epsilon^{-1/2}$. To see this, it is useful to rescale η_0 in terms of the capillary length, l_c. Using the relation $L/l_c = \epsilon^{1/2}$, we get

$$\frac{\tilde{\eta}_0}{l_c} = \frac{\tilde{\eta}_0}{L}\epsilon^{1/2}. \tag{4.29}$$

In the limit $\epsilon \to 0$, we expect the meniscus shape to approach that corresponding to a clean interface where elasticity is absent. According to (3.26), which was derived with $\epsilon = 0$, we get $\tilde{\eta}_0/l_c = \sqrt{2}$. We thus require $\tilde{\eta}_0/L \to \epsilon^{-1/2}$ to negate the ϵ dependence as $\epsilon \to 0$. At the other extreme where $\epsilon \to \infty$, we expect $\eta_0 \to \epsilon^{-1/4}$. To again see this, we use the relation $L/l_e = \epsilon^{1/4}$, thus

$$\frac{\tilde{\eta}_0}{l_e} = \frac{\tilde{\eta}_0}{L}\epsilon^{1/4}. \tag{4.30}$$

As shown in Dixit & Homsy (2013), in the pure elasticity problem where surface tension is neglected, we get $\tilde{\eta}_0/l_e = 1.7358$. To be consistent with this result, we require $\tilde{\eta}_0/L \to \epsilon^{-1/4}$ as $\epsilon \to \infty$. The power laws shown in figure 5(*a*), obtained by curve fitting, are broadly consistent with these limiting cases. Owing to the convex
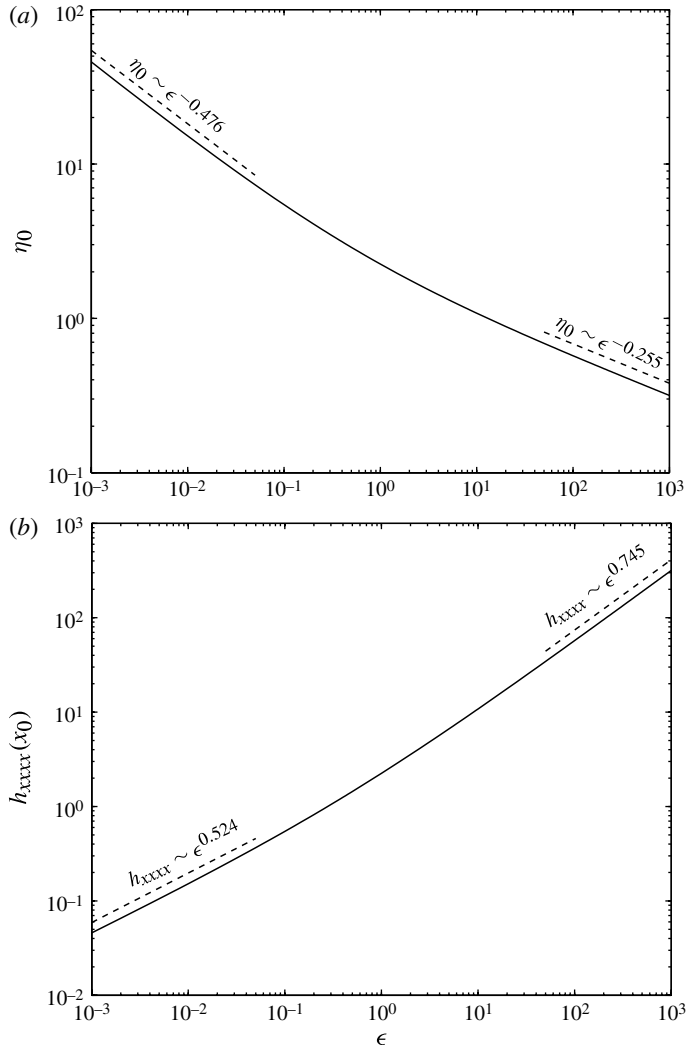
FIGURE 5. (a) The location of the apparent contact line, η_0, and (b) h_{xxxx} at the contact line as a function of ϵ. The dashed lines show fits taken for $\epsilon \leqslant 10^{-2}$ and $\epsilon \geqslant 10^2$. In (a) and (b), the expected power-law exponents are $-1/2$ and $1/2$ respectively in the limit of $\epsilon \to 0$, and $-1/4$ and $3/4$ in the limit of $\epsilon \to \infty$.

shape of the curve, we expect these power laws to approach the limiting cases $\sim \epsilon^{-1/2}$ and $\sim \epsilon^{-1/4}$ as $\epsilon \to 0$ and ∞ respectively.

Since $h_{xxxx}(x_0) = 24c_0$ where $c_0 = 1/d^4$, we get from (4.28) $h_{xxxx}(x_0) = \epsilon \eta_0$. Therefore the limiting behaviours for $h_{xxxx}(x_0)$ as $\epsilon \to 0$ and ∞ are $\sim \epsilon^{1/2}$ and $\sim \epsilon^{3/4}$ respectively. Again, the curve fits shown in figure 5(b) are consistent with these values. To further verify if the limiting behaviour is truly obeyed as $\epsilon \to 0$ and ∞, we directly compare the shape of the static meniscus obtained by solving (4.19) with the limiting cases $\epsilon = 0$ and $1/\epsilon = 0$. In the former case, the relevant length scale is the capillary length, l_c, and the comparison is shown in figure 6(a) where we set $\epsilon = 10^{-3}$. In the latter case, the relevant length scale is the elasticity length, l_e, and the comparison
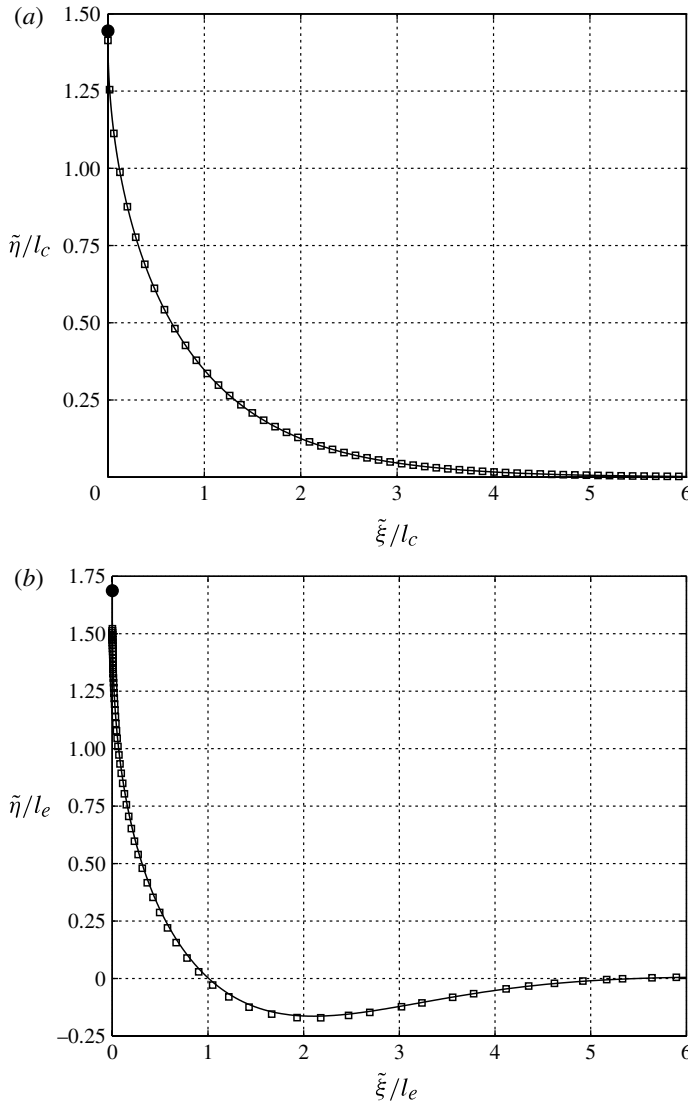
FIGURE 6. (*a*) Shape of the static interface shown with a solid line rescaled in terms of capillary length, l_c, for $\epsilon = 10^{-3}$. The symbols correspond to the exact solution given in (3.26). (*b*) Shape of the static interface shown with a solid line rescaled in terms of elasticity length, l_e for $\epsilon = 10^3$. The symbols correspond to the shape of an elastic meniscus given in Dixit & Homsy (2013). The black circle shows the location of the contact line.

is shown in figure 6(*b*) where we set $\epsilon = 10^3$. It is clear from these figures that the agreement between limiting static shapes and intermediate static shapes calculated at finite but small (or large) ϵ is excellent. This further validates the solution procedure adopted in §4.4. The shape of the static interface for various values of ϵ is shown in figure 7. As discussed earlier the structure of the solution and decay rates widely differ with varying ϵ.

We now show that the cubic term in (4.12) also vanishes by analysing higher-order effects in the static problem. This puts a constraint on the far-field nature of the
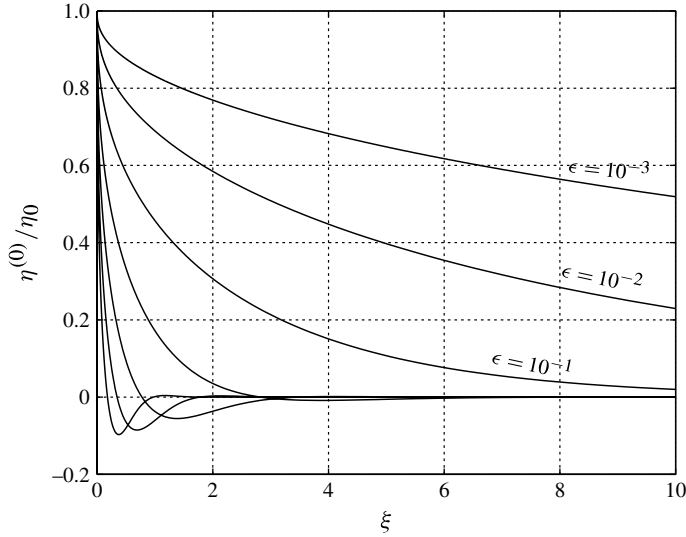
FIGURE 7. Shape of a static interface for $\epsilon = 10^{-3}, 10^{-2}, 10^{-1}, 1, 10, 10^2, 10^3$. The interface shape exhibits an oscillatory decay for $\epsilon < 1/4$.

solution of the transition region. It can be shown that the $O(Ca^{1/7})$ correction to the static shape identically vanishes for all ϵ. Since viscous terms do not contribute at $O(Ca^{1/7})$, and no new additional terms arise at this order, corrections to the interface shape can only arise from modifications to the boundary conditions at $x = x_0$. We can show that x_0 is independent of Ca by analysing the $O(Ca^{1/7})$ correction to the static equation (4.19) as discussed in §4 of Dixit & Homsy (2013) in greater detail. This leads to the conclusion that $c_1 = 0$, and hence the cubic term in (4.12) is absent.

4.6. *Solution: transition region*

Since $c_1 = 0$, we can use (4.12) to impose two boundary conditions as $\bar{x} \to -\infty$. For numerical purposes, we integrate (4.9) from $x_{max} = 0$ to $x_{min} = -100$. We rewrite the transition region equation with relevant boundary conditions for convenience:

$$\bar{h}^{(0)}_{\bar{x}\bar{x}\bar{x}\bar{x}} = \frac{3(\bar{h}^{(0)} - \bar{h}^{(0)}_\infty)}{(\bar{h}^{(0)})^3}, \tag{4.31a}$$

with

$$\bar{h}^{(0)} = \bar{h}^{(0)}_\infty + Ae^{\lambda_r \bar{x}}\cos(\lambda_i \bar{x}) \quad \text{and its derivatives at } \bar{x} = x_{max}, \tag{4.31b}$$

$$\left.\begin{array}{l} \bar{h}^{(0)}_{\bar{x}\bar{x}\bar{x}\bar{x}} = 24c_0 \\ \bar{h}^{(0)}_{\bar{x}\bar{x}\bar{x}} = 24c_0 x_{min} \end{array}\right\} \quad \text{at } \bar{x} = x_{min}. \tag{4.31c}$$

We drop the superscript (0) for convenience. Since $h_{xxxx}(x_0)$, and hence c_0, is known, the boundary value formulation of the transition region problem is now complete. As shown in figure 5(b), $h_{xxxx}(x_0)$ is a function of ϵ and hence the film thickness $\bar{h}_\infty$ is affected by surface tension.

We solve (4.31) using MATLAB's *bvp4c* solver in all our calculations. For a given ϵ, the parameters A and $\bar{h}_\infty$ are varied, keeping the domain of integration fixed in the range $[0, -100]$. Remarkably, five different solutions are obtained for each value
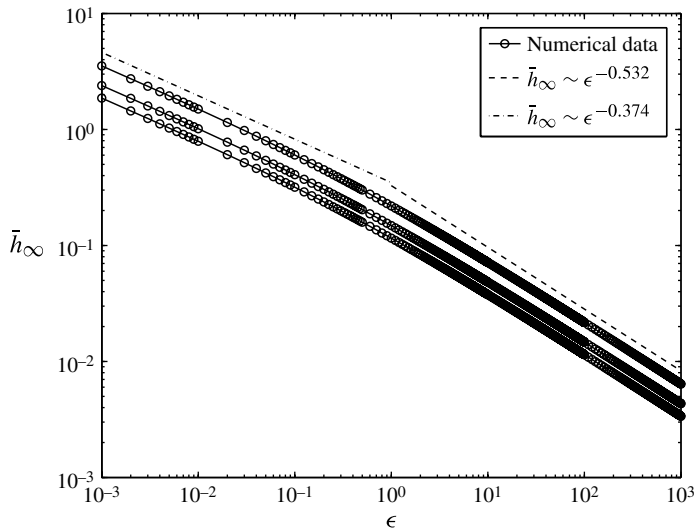
FIGURE 8. Variation of film thickness with the elastocapillary number. The three curves show three different families of solutions to (4.31) and the dashed and dashed-dotted lines show power-law fits taken with $\epsilon \geqslant 10^2$ and $\epsilon \leqslant 10^{-2}$ respectively.

of ϵ. The detailed numerical procedure for finding multiple solutions is outlined in Dixit & Homsy (2013) and we do not repeat it here. Since ϵ is a free parameter, the five solutions are really five one-parameter families of solutions. We show three of these branches in figure 8. It is clear from figure 8 that except for a constant multiplying factor, the functional dependence of $\bar{h}_\infty$ on ϵ is the same for all the branches. This relationship can be written as

$$\bar{h}_\infty(\epsilon) = \bar{h}_{\infty,e} f(\epsilon), \tag{4.32}$$

where $f(\epsilon)$ represents the shape of the curves in figure 8, and $\bar{h}_{\infty,e}$, a number, is the film thickness in the limit $\epsilon \to \infty$ in the transition region. We show below that $\bar{h}_{\infty,e}$ is the numerical coefficient of the elastic Landau–Levich flow found in Dixit & Homsy (2013).

Consider the uppermost branch in figure 8. A power law fit for $\epsilon > 10^2$ gives us

$$\bar{h}_\infty = 0.2524\epsilon^{-0.532}. \tag{4.33}$$

Writing this expression in dimensional form, we get

$$\tilde{h}_\infty(\epsilon, Ca) = 0.2524 L \epsilon^{-0.532} Ca^{4/7}. \tag{4.34}$$

To understand this result, we need to take a closer look at the limiting case of $\epsilon \to \infty$. In this limit, the static solution reduces to the elastic meniscus solution of Dixit & Homsy (2013) as evident from figure 6(*b*). Moreover, the transition region equation, (4.31*a*), is independent of surface tension. We therefore expect the film thickness in the present problem to approach the purely elastic Landau–Levich solution in the limit $\epsilon \to \infty$. As shown in Dixit & Homsy (2013), in the absence of surface tension, the elastic Landau–Levich law in dimensional form can be written as

$$\tilde{h}_{\infty,e}(El) = \bar{h}_{\infty,e} l_e El^{4/7}, \tag{4.35}$$

Solution	A	$\bar{h}_{\infty,e}$
1	2.007×10^{-12}	0.0999
2	-1.7777×10^{-10}	0.1157
3	1.6483×10^{-8}	0.1390
4	-1.6594×10^{-6}	0.1783
5	2.0258×10^{-4}	0.2634

TABLE 1. List of solutions for the purely elastic Landau–Levich flow given in Dixit & Homsy (2013) obtained by solving (4.31) with $c_0 = 0.07232$, which corresponds to the value in the limit $\epsilon \to \infty$.

where $\bar{h}_{\infty,e}^{(0)}$ can assume one of five different values as given in table 1, and El is the elasticity number. Each solution is associated with a different value of A in (4.31). Consider the highest solution in this set, which can be written again as

$$\tilde{h}_{\infty,e} = 0.2634 l_e El^{4/7}$$
$$= 0.2634 L \left(\frac{l_e}{L} \right) \left(\frac{El}{Ca} \right)^{4/7} Ca^{4/7}$$
$$= 0.2634 L \epsilon^{-15/28} Ca^{4/7}. \tag{4.36}$$

Since $15/28 \approx 0.536$, the above expression is almost identical to (4.34) except for minor numerical differences which are understandable since (4.34) is obtained with $\epsilon \leqslant 10^3$ whereas (4.36) is obtained in the limit $\epsilon \to \infty$. The slightly concave shape of the curves in figure 8 makes it safe to assume that the limiting behaviour for $\epsilon \to \infty$ will approach the purely elastic Landau–Levich case studied in Dixit & Homsy (2013). Hence the correct form of the power-law scaling can be written as

$$\tilde{h}_{\infty,e} = \bar{h}_{\infty,e} L f(\epsilon) Ca^{4/7}. \tag{4.37}$$

This expression is valid for all values of ϵ through the shape function $f(\epsilon)$. This is the main result of this section, and it establishes the relationship between the film thickness and a combination of mechanical properties of the interface and dynamic flow conditions. Since $Ca = \mu U / \sigma$, the film thickness varies with the plate speed as $U^{4/7}$.

Let us now examine the other limit of $\epsilon \to 0$. This is the limit of weak elasticity and hence the film thickness is expected to be a function of surface tension, viscosity and gravity, which is the regime of validity of the classical Landau–Levich law for a clean interface,

$$\tilde{h}_{\infty,c} = 0.9458 l_c Ca^{2/3}. \tag{4.38}$$

According to the above relation, the film thickness in the Landau–Levich law varies as $U^{2/3}$, which differs from the $U^{4/7}$. Therefore it is not possible for (4.37) to agree with (4.38) using any transformation in the length scales. This suggests that there exists an additional regime with small ϵ where a simple power-law asymptotic expansion in Ca is not possible. A detailed investigation of this regime which connects the elastocapillary regime studied here to the classical Landau–Levich regime is beyond the scope of this paper.

5. Note on the weak surface tension regime

Analogously to the weak elasticity regime studied in § 3, it is also possible to study the effect of weak surface tension on the elastic Landau–Levich flow. In this regime, the elastocapillary number ϵ is large. The relevant length scale in this regime is the elasticity length, l_e. Rescaling pressure with K_B/l_e^3, the hydrostatic force balance and the normal stress balance equations become

$$p_x = -1, \tag{5.1a}$$

$$p = \frac{-1}{\epsilon^{1/2}} \frac{h_{xx}}{(1+h_x^2)^{3/2}} + \frac{2(1+h_x^2)^2 h_{xxxx} - 20(1+h_x^2)h_x h_{xx} h_{xxx} - 5(1-6h_x^2)h_{xx}^3}{2(1+h_x^2)^{9/2}}. \tag{5.1b}$$

To obtain the transition region scaling, we balance elasticity with viscous forces in the inner region and use the lubrication approximation (see Dixit & Homsy 2013 for more details). The scalings can be written as

$$(\bar{x}, \bar{y}) = \left(\frac{x - x_0}{El^{1/7}}, \frac{y}{El^{4/7}} \right), \tag{5.2a}$$

$$(\bar{u}, \bar{v}) = \left(u, \frac{v}{El^{3/7}} \right), \tag{5.2b}$$

$$\bar{p} = p, \quad \bar{h} = \frac{h}{El^{4/7}}. \tag{5.2c}$$

The normal stress balance equation in the transition region becomes

$$p = -\frac{El^{2/7}}{\epsilon^{1/2}} \bar{h}_{\bar{x}\bar{x}} + \bar{h}_{\bar{x}\bar{x}\bar{x}\bar{x}}. \tag{5.3}$$

Solving for the velocity field from the momentum equation and using the same procedure used in §§ 3 and 4, a single nonlinear differential equation can be obtained for the film thickness, $\bar{h}(\bar{x})$,

$$\bar{h}_{\bar{x}\bar{x}\bar{x}\bar{x}} - \frac{El^{2/7}}{\epsilon^{1/2}} \bar{h}_{\bar{x}\bar{x}} = \frac{3(\bar{h} - \bar{h}_\infty)}{\bar{h}^3}. \tag{5.4}$$

We are interested in the regime where $El \ll 1$ and $\epsilon \gg 1$. Therefore $El^{2/7}/\epsilon^{1/2}$ is smaller than $1/\epsilon^{1/2}$, hence we use $\beta = El^{2/7}/\epsilon^{1/2}$ as the small parameter. We now carry out a double expansion in the small parameters $El^{1/7}$ and β. Writing the expansion for $\bar{h}$ to first-order terms, we get

$$\bar{h} = \bar{h}^{00} + El^{1/7}\bar{h}^{01} + \beta\bar{h}^{10} + \cdots, \tag{5.5}$$

where the first superscript corresponds to the β correction and the second one to the $El^{1/7}$ correction. The sequential ordering of terms in the above expansion depends on the relative size of β and $El^{1/7}$. If $\epsilon \gg 1$, clearly $\beta \ll El^{1/7}$. This is true even when $\epsilon \sim O(1)$. Therefore the first β correction is actually a second-order effect. As discussed in Dixit & Homsy (2013), a gravitational correction to the purely elastic Landau–Levich flow arises at $O(El^{1/7})$. In this paper, we are only interested in evaluating first-order effects and therefore do not evaluate the small-β effects any further.

6. Summary and discussion

In this paper, we have developed a theory of dip-coating flows where the interface is governed by a combination of elasticity and surface tension. The present paper is

Landau–Levich and weak elasticity regimes	Simple power-law expansion not valid in this region	Elastocapillary Landau–Levich regime	Elastic Landau–Levich and strong elasticity regimes
$h_\infty \sim U^{2/3}$	h_∞ transitions from $U^{2/3}$ to $U^{4/7}$	$h_\infty \sim U^{4/7}$	$h_\infty \sim U^{4/7}$
Single solution		Multiple solutions	Multiple solutions
$\epsilon \ll O[Ca^{2/3}]$	$O[Ca^{2/3}] \sim \epsilon \ll 1$	$\epsilon \sim O(1)$	$\epsilon \gg 1$

FIGURE 9. All possible regimes in the Landau–Levich dip-coating flow where the interface possesses surface tension and/or elasticity.

a continuation of the elastic Landau–Levich flow theory developed in Dixit & Homsy (2013) where surface tension was absent. Analogously to the classical Landau–Levich flow, the flow field can be divided into three separate regions: (i) the outer or static region far away from the plate where the interface shape is dictated by a balance of gravity, elasticity and/or surface tension; (ii) the inner or transition region near the plate where the interface shape is dictated by a balance of viscous forces, elasticity and/or surface tension; and (iii) a thin-film region on the surface of the plate where the flow is uniform and tangential to the moving plate.

Because of the presence of a new physical effect, the elasticity of the interface, the physics of film formation is now dictated by the relative balance of gravity, viscosity, elasticity and surface tension. Elasticity further introduces an additional length scale, $l_e = (K_B/\rho g)^{1/4}$, into the problem. This elasticity length scale is analogous to the well-known capillary length scale for a hydrostatic interface with surface tension.

Based on the relative strengths of elasticity and surface tension, various flow regimes are possible. This is facilitated by defining an elastocapillary number, $\epsilon = K_B/\sigma l_c^2$, which is physically the ratio of energy cost associated with deforming an interface with elasticity and surface tension respectively. To gain a complete understanding of the role of elasticity in the dip-coating process, we study the entire range of ϵ from zero to infinity. We identify three main regimes based on the size of ϵ as shown schematically in figure 9.

(i) In the limit of vanishing ϵ where $\epsilon \ll O(Ca^{2/3})$, elasticity is weak relative to surface tension. Hence the relevant length scale in this regime is the capillary length, l_c. At leading order, the flow is identical to the classical Landau–Levich flow. With weak elasticity, we show that the shape of the fluid interface is marginally altered and that elasticity causes film thinning relative to the classical Landau–Levich case. The resultant power-law scaling can be written as

$$\tilde{h}_{\infty,c} = (0.9458 - 0.0839 \; \mathscr{E})l_c Ca^{2/3}. \tag{6.1}$$

(ii) When ϵ is very large, elasticity dominates over surface tension effects. If surface tension is neglected, we arrive at the elastic Landau–Levich flow, which was studied in detail in our previous paper, Dixit & Homsy (2013). A remarkable feature of this regime is the presence of multiple solutions. The resultant power-law scaling can be written as

$$\tilde{h}_{\infty,e} = \bar{h}_{\infty,e} l_e El^{4/7}, \tag{6.2}$$

where we find five different values for the numerical coefficient $\bar{h}_{\infty,e}$. This regime can at least be extended to study the case of weak surface tension. It is shown that weak surface tension is a second-order effect and is therefore not pursued in this paper.

(iii) Between the above two regimes, we have the elastocapillary regime where $\epsilon \sim O(1)$, i.e. elasticity and surface tension are of comparable magnitude. In this regime, the natural length scale is the so-called elastocapillary length, $L = (K_B/\sigma)^{1/2}$. In this regime, it is shown that surface tension affects only the static interface shape and is completely absent in the transition region. The resultant power-law scaling for the film thickness takes the form

$$\tilde{h}_{\infty,ec} = \bar{h}_{\infty,e} L f(\epsilon) Ca^{4/7}, \qquad (6.3)$$

where $f(\epsilon)$ is the functional dependence of the film thickness on ϵ as shown in figure 8.

The above three power laws, (6.1)–(6.3), are the main results of Dixit & Homsy (2013) and of this paper. We further show that (6.3) in the elastocapillary regime approaches (6.2) in the elastic regime in the limit of $\epsilon \to 0$. But no such matching was possible between (6.3) and (6.1). The two power laws possess a different exponent for the capillary number. Therefore a simple power-law expansion cannot be found which takes the scaling from (6.1) to (6.3). Therefore there exists a hidden region, shown by the shaded region in figure 9, where the film thickness transitions from $Ca^{2/3}$ to $Ca^{4/7}$, or in terms of velocity, from $U^{2/3}$ to $U^{4/7}$.

Except for a small region where $O(Ca^{2/3}) \lesssim \epsilon \ll 1$, the present paper along with its companion, Dixit & Homsy (2013), presents a complete theory of the Landau–Levich dip-coating flow for an interface with surface tension and/or elasticity.

As discussed in the introduction, there has been a great deal of interest in recent years in understanding the role of elasticity in various interfacial flow problems. The present problem contributes to this growing literature on elastocapillary flows by addressing the role of elasticity in one of the most fundamental fluid dynamical problems, namely the Landau–Levich dip-coating flow.

In a recent experiment of Ouriemi & Homsy (2013), it was shown that small surface-adsorbed hydrophobic particles alter the dip-coating process in the following ways: first, particles lead to film thickening relative to the cleaner cousin, and second, the power-law scaling of film thickness with velocity of the plate is altered from the classical $U^{2/3}$ to $U^{0.57}$. It is interesting to note that if elasticity is included as an $O(1)$ effect, the scaling obtained is $U^{4/7}$ as shown in figure 9, which is strikingly close to the experimental observation. This suggests that elasticity played a role in the experiments of Ouriemi & Homsy (2013). A detailed comparison between the scaling law (6.2) and experiments is presented in our companion paper, Dixit & Homsy (2013), where it is shown that the theoretical prediction differs only by a factor of two from the experimental observation. In order to make a quantitative comparison with the elastocapillary result, (6.3), the bending stiffness of the interface has to be measured. We hope the present theory motivates more experiments in this direction.

Within the frame of elastocapillary effects on low-speed flows, the present theory is highly simplified with many restrictions. The first of these is the limitation of constant surface tension and elasticity. If elasticity is indeed the result of surface species such as surfactants or colloidal particles, then it is natural to conceive that the material properties of the interface will be a direct function of the particle concentration. Therefore a natural extension of the present theory is to cases when both surface tension and elasticity vary along the interface. Such theories with Marangoni effects exist for dip-coating flows with variable surfactant concentration where elasticity is

neglected. In the case of elasticity, it would be interesting to know the role of elastic–Marangoni effects in interfacial flows. The second limitation of the present theory is the restriction on power-law asymptotic behaviour. As we have seen, the present theory fails to explain the variation in scaling from $U^{2/3}$ to $U^{4/7}$ in the small region sandwiched between the weak elasticity and elastocapillary regimes. A more generalized theory or numerical tools are required to uncover the physics in this region.

The presence of multiple solutions in the strong elasticity and elastocapillary regimes is intriguing, especially since the weak elasticity problem does not exhibit such behaviour. This suggests that a bifurcation is expected to occur in the shaded region of figure 9. Such a bifurcation would of course vanish if a unique solution could be found from the family of multiple solutions found here. Therefore a pressing issue for future study concerns the stability of these multiple solutions.

In spite of the above simplicity, the present theory reveals the possibility of rich dynamics in other interfacial flows with interfacial elasticity.

Acknowledgements

Appendix. Absence of an intermediate asymptotic regime

In § 3, we investigated the effect of elasticity on the Landau–Levich flow in the limit when elasticity was weak in relation to surface tension. This was made possible by assuming that $\mathscr{E} \ll 1$, equivalently written as $\epsilon \ll Ca^{2/3}$. A natural extension of this regime would be to assume that $\epsilon \sim O(Ca^{2/3})$, i.e. $\mathscr{E} \sim O(1)$. The leading-order normal stress balance equation in the static region, (3.11b), now becomes (omitting the superscript for convenience)

$$p + \frac{h_{xx}}{\left(1 + (h_x)^2\right)^{3/2}} = 0, \tag{A 1}$$

which is identical to the zero-elasticity Landau–Levich case discussed earlier. Hence elasticity does not determine the shape of the static meniscus in this regime. Similarly, the normal stress balance equation (3.15b) written in the transition region in terms of $\mathscr{E}$ becomes

$$\bar{p} + \bar{h}_{\bar{x}\bar{x}} - \mathscr{E}\bar{h}_{\bar{x}\bar{x}\bar{x}\bar{x}} = 0. \tag{A 2}$$

Since $\mathscr{E} \sim O(1)$, both elasticity and surface tension effects are of comparable magnitude in the transition region. Solving for the velocity field from the momentum equation and relating the pressure gradient to the viscous stresses, we obtain a single equation for the film thickness, $\bar{h}(\bar{x})$, as

$$\mathscr{E}\bar{h}_{\bar{x}\bar{x}\bar{x}\bar{x}\bar{x}} - \bar{h}_{\bar{x}\bar{x}\bar{x}} = \frac{3(\bar{h} - \bar{h}_\infty)}{\bar{h}^3}. \tag{A 3}$$

This equation is analogous to the Landau–Levich equation derived earlier. As $\bar{x} \to -\infty$, $\bar{h}$ becomes large, hence the asymptotic behaviour of (A 3) becomes

$$\bar{h}(\bar{x}) = \mathscr{E}^{3/2}(Ae^{\bar{x}/\mathscr{E}} + Be^{-\bar{x}/\mathscr{E}}) + C_0\bar{x}^2 + C_1\bar{x} + C_2. \tag{A 4}$$
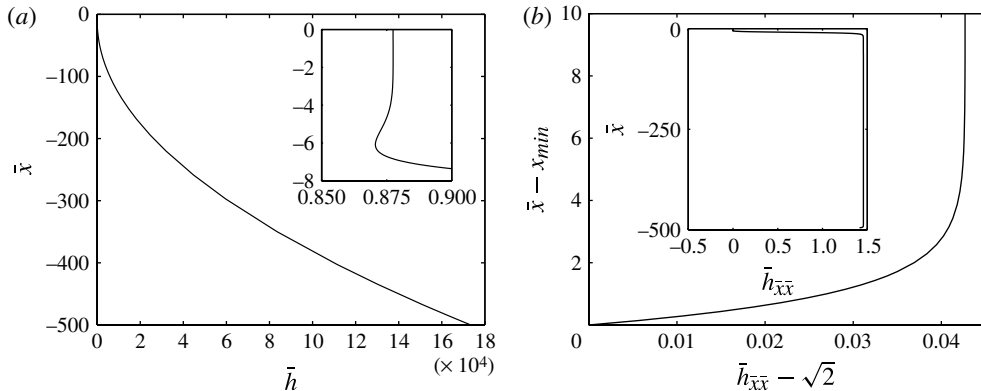
FIGURE 10. (*a*) Solution of (A 3) obtained with $\mathscr{E} = 1$. The inset is a close-up view of the solution which reveals a dimple structure. (*b*) Boundary layer structure of curvature at the lower end of the integration domain. The inset shows curvature throughout the domain.

The exponentially decaying term becomes insignificant when $\bar{x}$ becomes large and negative so that

$$\bar{h}(\bar{x}) = C_0\bar{x}^2 + C_1\bar{x} + C_2 \quad \text{as } \bar{x} \to -\infty. \tag{A 5}$$

The matching conditions are identical to (3.25), but now valid for an $O(1)$ value for $\mathscr{E}$. Since the static equation (A 1) and the corresponding matching conditions at the plate remain unaltered, the shape of the static meniscus is identical to (3.26) obtained earlier. Moreover, the value of C_0 is fixed at $1/\sqrt{2}$. We now solve (A 3) iteratively from $x_{max} = 0$ to $x_{min} = -500$ as a boundary value problem. The boundary conditions at $x = x_{min}$ can be written as

$$\left.\begin{array}{l} \bar{h}_{\bar{x}\bar{x}} = 2C_0 \\ \bar{h}_{\bar{x}\bar{x}\bar{x}} = 0 \end{array}\right\} \quad \text{at } \bar{x} = x_{min}. \tag{A 6}$$

Additional boundary conditions are imposed at $x = x_{max}$ by linearizing (A 3) about $\bar{h} = \bar{h}_\infty$. We varied $\mathscr{E}$ over a wide range of values and the solution for one particular value is shown in figure 10. Figure 10(*a*) reveals no surprises and yields a film thickness of $\bar{h}_\infty = 0.877$. A closer examination near the lower end of the domain where (A 6) is imposed reveals a boundary layer structure (figure 10*b*). Such a solution structure was found for all values of $\mathscr{E}$ and with different values for x_{min}. This exposes a fundamental deficiency in the problem formulation and shows that there is no solution in the asymptotic regime where $\epsilon \sim O(Ca^{2/3})$.

REFERENCES

BICO, J., ROMAN, B., MOULIN, L. & BOUDAOUD, A. 2004 Elastocapillary coalescence in wet hair. *Nature* **432**, 690.

BRETHERTON, F. P. 1961 The motion of long bubbles in tubes. *J. Fluid Mech.* **10**, 166–188.

DAS, S., MARCHAND, A., ANDREOTTI, B. & SNOEIJER, J. H. 2011 Elastic deformation due to tangential capillary forces. *Phys. Fluids* **23**, 072006.

DIXIT, H. N. & HOMSY, G. M. 2013 The elastic Landau–Levich problem. *J. Fluid Mech.* **732**, 5–28.

DUPRAT, C., ARISTOFF, J. M. & STONE, H. A. 2011 Dynamics of elastocapillary rise. *J. Fluid Mech.* **679**, 641–654.

KAOUI, B., RISTOW, G. H., CANTAT, I., MISBAH, C. & ZIMMERMANN, W. 2008 Lateral migration of a two-dimensional vesicle in unbounded Poiseuille flow. *Phys. Rev.* E **77**, 021903.

KIM, H.-Y. & MAHADEVAN, L. 2006 Capillary rise between elastic sheets. *J. Fluid Mech.* **548**, 141–150.

OURIEMI, M. & HOMSY, G. M. 2013 Experimental study of the effect of surface-adsorbed hydrophobic particles on the Landau–Levich law. *Phys. Fluids* **25**, 082111.

PARK, C.-W. 1991 Effects of insoluble surfactants on dip coating. *J. Colloid Interface Sci.* **146**, 382–394.

PARK, C.-W. & HOMSY, G. M. 1984 Two-phase displacement in Hele-Shaw cells: theory. *J. Fluid Mech.* **139**, 291–308.

PIHLER-PUZOVIĆ, D., ILLIEN, P., HEIL, M. & JUEL, A. 2012 Suppression of complex fingerlike patterns at the interface between air and a viscous fluid by elastic membranes. *Phys. Rev. Lett.* **108**, 074502.

PLANCHETTE, C., LORENCEAU, E. & BIANCE, A.-L. 2012 Surface wave on a particle raft. *Soft Matt.* **8**, 2444–2451.

PY, C., REVERDY, P., DOPPLER, L., BICO, J., ROMAN, B. & BAROUD, C. N. 2007 Capillary origami: spontaneous wrapping of a droplet with an elastic sheet. *Phys. Rev. Lett.* **98**, 156103.

SEIFERT, U. 1995 The concept of effective tension for fluctuating vesicles. *Z. Phys.* B **97**, 299–309.

VAN DYKE, M. D. 1975 *Perturbation Methods in Fluid Mechanics*. Parabolic Press.

VELLA, D., AUSSILLOUS, P. & MAHADEVAN, L. 2004 Elasticity of an interfacial particle raft. *Europhys. Lett.* **68**, 212–218.

WILSON, S. D. R. 1982 The drag-out problem in film coating theory. *J. Engng Maths* **16**, 209–221.